July 11, 2013

Theoretical Basis for the Empirical Green's Function Method

1. The empirical Green's function method by Irikura (1983)

The starting point for the formulation of the empirical Green's function method is the expression for the far-field displacement waveform for a homogeneous elastic media. By taking the far-field S term of the expression for the displacement waveform such as in equation (4.32) of Aki and Richards (2002), one obtains

$$\mathbf{u}(\mathbf{x},t) = \frac{\mu \mathbf{R}^{FS}}{4\pi\rho\beta^3}\frac{1}{r}\dot{D}\left(t-\frac{r}{\beta}\right)S \tag{1}$$

where ρ is the density, μ is the rigidity, β is the S wave velocity, $\mathbf{R}^{FS}$ is the radiation coefficient for the far-field S term, r is the distance from the source to the site, $\dot{D}(t)$ is the slip velocity time function, and S is the area of the source. For a finite source, that is, a source that cannot be regarded as a point source, by integrating the right hand side of Equation (1) over the area of the finite source, one obtains

$$\mathbf{u}(\mathbf{x},t) = \frac{\mu \mathbf{R}^{FS}}{4\pi\rho\beta^3}\iint \frac{1}{r}\dot{D}\left(t-\frac{|\boldsymbol{\xi}|}{v_r}-\frac{r}{\beta}\right)dS \tag{2}$$

where $|\boldsymbol{\xi}|$ is the distance from the rupture starting point to an arbitrary point on the fault, r is the distance from an arbitrary point on the fault to the site, and $\dot{D}(t)$ is the slip velocity time function at the rupture starting point. In Equation (2), the slip velocity time function is assumed to be uniform over the fault, except for the time shift due to radial rupture propagation with a velocity v_r. Parameters such as ρ, μ, β, and $\mathbf{R}^{FS}$ are assumed to be uniform over the fault plane and put outside the integration sign.

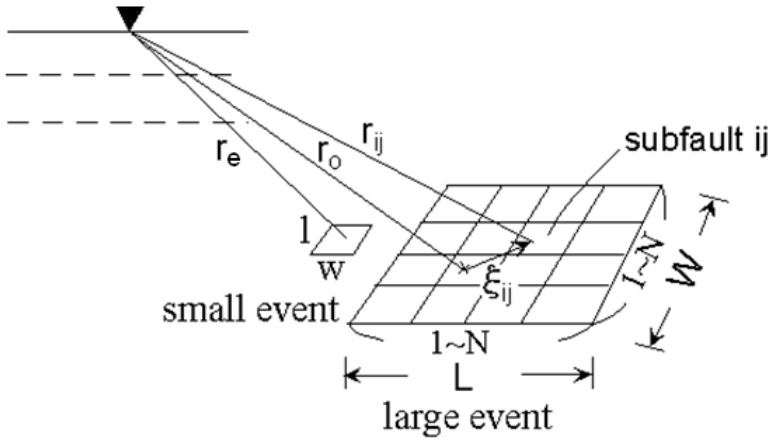

Figure 1 In the empirical Green's function method, the fault of a large event with length L and width W is discretized into N×N subfaults. Then, a small event that occurs near the large event and has the same area as the subfault of the large event is considered. In the figure, ξ_{ij} denotes the distance from the rupture starting point to the (i, j) subfault. r_{ij} denotes the distance from the (i, j) subfault to the site. r_e denotes the distance from the small event to the site.

Now we restrict ourselves to a rectangular fault as shown in Figure 1 and discretize it into $N_L \times N_W$ subfaults. Then the displacement waveform can be approximated by

$$\mathbf{u}(\mathbf{x},t) = \frac{\mu \mathbf{R}^{FS}}{4\pi\rho\beta^3} \sum_{i=1}^{N_L} \sum_{j=1}^{N_W} \frac{1}{r_{ij}} \dot{D}\left(t - \frac{\xi_{ij}}{v_r} - \frac{r_{ij}}{\beta}\right) \Delta L \Delta W \tag{3}$$

where ξ_{ij} denotes the distance from the rupture starting point to the (i, j) subfault; r_{ij} denotes the distance from the (i, j) subfault to the site.

Then the slip velocity time function $\dot{D}(t)$ is assumed to be uniform over the time $0 \sim \tau_r$, where τ_r is the rise time, and it is discretized as shown in Fugure 2 and Equation (4).

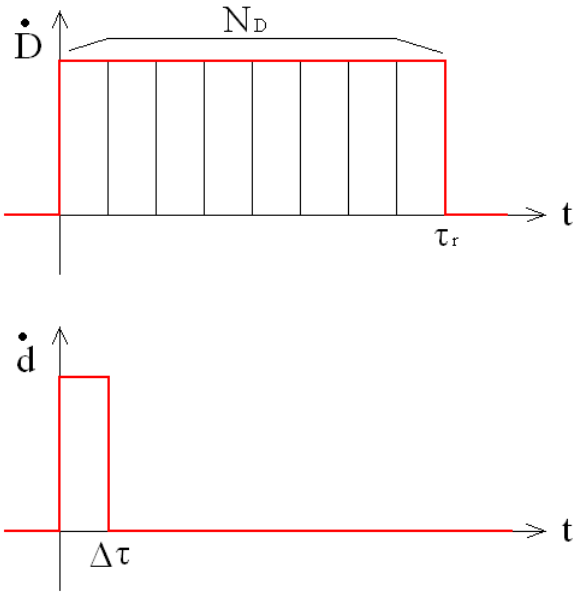

Figure 2 Slip velocity time functions for a large event (top) and a small event (bottom).

$$\dot{D}(t) = \sum_{k=1}^{N_D} \dot{d}(t - (k-1)\Delta\tau) \tag{4}$$

From equations (3) and (4), one obtains

$$\mathbf{u}(\mathbf{x},t) = \frac{\mu \mathbf{R}^{FS}}{4\pi\rho\beta^3} \sum_{i=1}^{N_L} \sum_{j=1}^{N_W} \sum_{k=1}^{N_D} \frac{1}{r_{ij}} \dot{d}\left(t - \frac{\xi_{ij}}{v_r} - \frac{r_{ij}}{\beta} - (k-1)\Delta\tau\right) \Delta L \Delta W \tag{5}$$

One the other hand, the displacement waveform for the small event shown in Figure 1 can be expressed as

$$\mathbf{u_e}(\mathbf{x},t) = \frac{\mu \mathbf{R}^{FS}}{4\pi\rho\beta^3}\frac{1}{r_e}\dot{d}\left(t-\frac{r_e}{\beta}\right)\Delta L\Delta W \tag{6}$$

where r_e denotes the distance from the small event to the site.

Equations (5) and (6) yields the relation between the waveforms for a large and an small events as

$$\mathbf{u}(\mathbf{x},t) = \sum_{i=1}^{N_L}\sum_{j=1}^{N_W}\sum_{k=1}^{N_D}\frac{r_e}{r_{ij}}\mathbf{u_e}\left(\mathbf{x}, t-\frac{\xi_{ij}}{v_r}-\frac{r_{ij}-r_e}{\beta}-(k-1)\Delta\tau\right) \tag{7}$$

This is the basic equation for the empirical Green's function method proposed by Irikura (1983). Equations (5) and (6) are the expressions for the waveforms for a homogeneous elastic media, that is, the waveforms before affected by the complexity of the media. If, however, one can assume that the heterogeneity of the media along the propagation path has the same effect on the waveforms for the large and small events, Equation (7) is still valid for the waveforms for a complex heterogeneous media. This is the idea for the empirical Green's function method.

By the way, Equation (7) can also be expressed as

$$\mathbf{u}(\mathbf{x},t) = \mathbf{u_e}(\mathbf{x},t) * F(t) * \sum_{i=1}^{N_L}\sum_{j=1}^{N_W}\frac{r_e}{r_{ij}}\delta(t-t_{ij}) \tag{8}$$

where * denotes convolution and

$$F(t) = \sum_{k=1}^{N_D}\delta(t-(k-1)\Delta\tau) \tag{9}$$

$$t_{ij} = \frac{\xi_{ij}}{v_r}+\frac{r_{ij}-r_e}{\beta} \tag{10}$$

$F(t)$ is the correction function for the difference of the slip velocity time functions between the large and the small events. By convolving $\mathbf{u_e}(\mathbf{x},t)$ with $F(t)$, one can correct for the difference of the slip velocity time functions (or the difference of the final slip) (Step1). Then, by convolving the result with

$$\sum_{i=1}^{N_L}\sum_{j=1}^{N_W}\frac{r_e}{r_{ij}}\delta(t-t_{ij})$$

one can sum up contributions from the subfaults (Step2).

2. Waveform inversion with empirical Green's functions

Equation (7) could be used with a weight w_{ijk} for each subfault and for each time window:

$$\mathbf{u}(\mathbf{x},t)=\sum_{i=1}^{N_L}\sum_{j=1}^{N_W}\sum_{k=1}^{N_D} w_{ijk}\frac{r_e}{r_{ij}}\mathbf{u_e}\left(\mathbf{x},t-\frac{\xi_{ij}}{v_r}-\frac{r_{ij}-r_e}{\beta}-(k-1)\Delta\tau\right) \tag{11}$$

When we have observed waveforms for a large event, w_{ijk} could be determine so that the synthetic waveforms best fit the observed ones. This is the waveform inversion with empirical Green's functions (e.g., Nozu and Irikura, 2008).

3. ω^{-2} model (Aki, 1967)

According to the ω^{-2} model (Aki, 1967), the displacement source spectrum $S(f)$ can be expressed as follows (for example, Equation (10.38) of Aki and Richards (2002)).

$$S(f)=\frac{S(0)}{1+(f/f_c)^2} \tag{12}$$

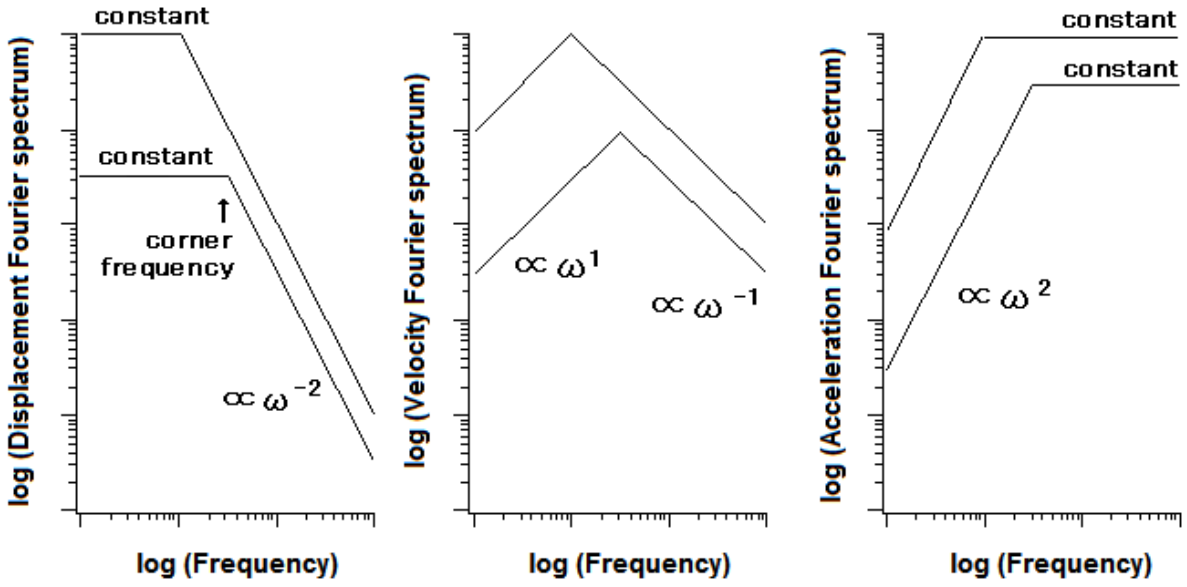

Figure 3 Displacement (left), velocity (center) and acceleration (right) source spectra following the ω^{-2} model (Aki, 1967).

The displacement, velocity and acceleration source spectra following the ω^{-2} model (Aki, 1967) are schematically illustrated in Figure 3.The displacement source spectrum is flat at low frequencies and the flat level $S(0)$ is proportional to seismic moment M_0. At frequencies higher than the corner frequency, which is dependent on the size of the earthquake, the displacement source spectrum is proportional to ω^{-2}, expressed as a straight line with a slope of -2 in

the double-logarithmic plot. The velocity source spectrum is proportional to ω^1 at low frequencies and is proportional to ω^{-1} at high frequencies. The acceleration source spectrum is proportional to ω^2 at low frequencies and is flat at high frequencies. The high frequency asymptote of the acceleration source spectrum is given by

$$\lim_{f\to\infty}(2\pi f)^2 S(f) = (2\pi f_c)^2 S(0) \tag{13}$$

As discussed in Section 10.1.5 of Aki and Richards (2002), the corner frequency is inversely proportional to either the size of the fault (note that the 'size' here indicates the length L or the width W, not the area) or the rise time τ_r. In addition, as discussed in Section 10.1.5 of Aki and Richards (2002), if we assume similarity between large and small earthquakes, the following relations hold.

$$L \propto W \propto \tau_r \propto M_0^{1/3} \tag{14}$$

Therefore, the corner frequency is inversely proportional to the size of the fault. To roughly express this relation, the following equation by Brune (1970, 1971) is often used.

$$f_c = \sqrt{7/16}\ \beta/\sqrt{S} = 0.66\ \beta/\sqrt{S} \tag{15}$$

where S stands for the area of the fault. Equation (15) is based on many assumptions and it cannot be regarded as a 'rigorous' equation that holds for any condition. The equation, however, is still valuable as a tool to roughly express the relation between the corner frequency and the size of the fault and is widely used in engineering seismology.

N.B. Based on the above discussion, if the ratio of the fault size is *n* between the large and the small event, the ratio of the seismic moment is n^3 and the ratio of the corner frequency is $1/n$. Therefore, the ratio of the low-frequency level is n^3, which is the ratio of $S(0)$, and that of the high frequency level is *n*, which is the ratio of $(2\pi f_c)^2 S(0)$.

4. The empirical Green's function method by Irikura (1986) and Irikura et al. (1997)

Based on the above discussion on the ω^{-2} model, it is preferable that the superposition operation of the empirical Green's functions amplify the low frequency-components by a factor of n^3 and the high-frequency components by a factor of *n* when the large and small events follow the relation expressed by Equation (14). Irikura (1983)'s superposition operation (Equation (8)-(10)) satisfies the former constraint but not the latter. So, Irikura (1986) proposed a new superposition method that satisfies both constraints, which was further revised by Irikura et al. (1997).

Instead of the correction function in Equation (9), Irikura (1986)'s superposition method uses

$$F(t) = \delta(t) + \frac{1}{n'}\sum_{k=1}^{(N_D-1)n'} \delta(t - t_k) \tag{16}$$

where *n*' is a sufficiently large integer and

$$t_k = \frac{(k-1)\tau_r}{(N_D - 1)n'} \tag{17}$$

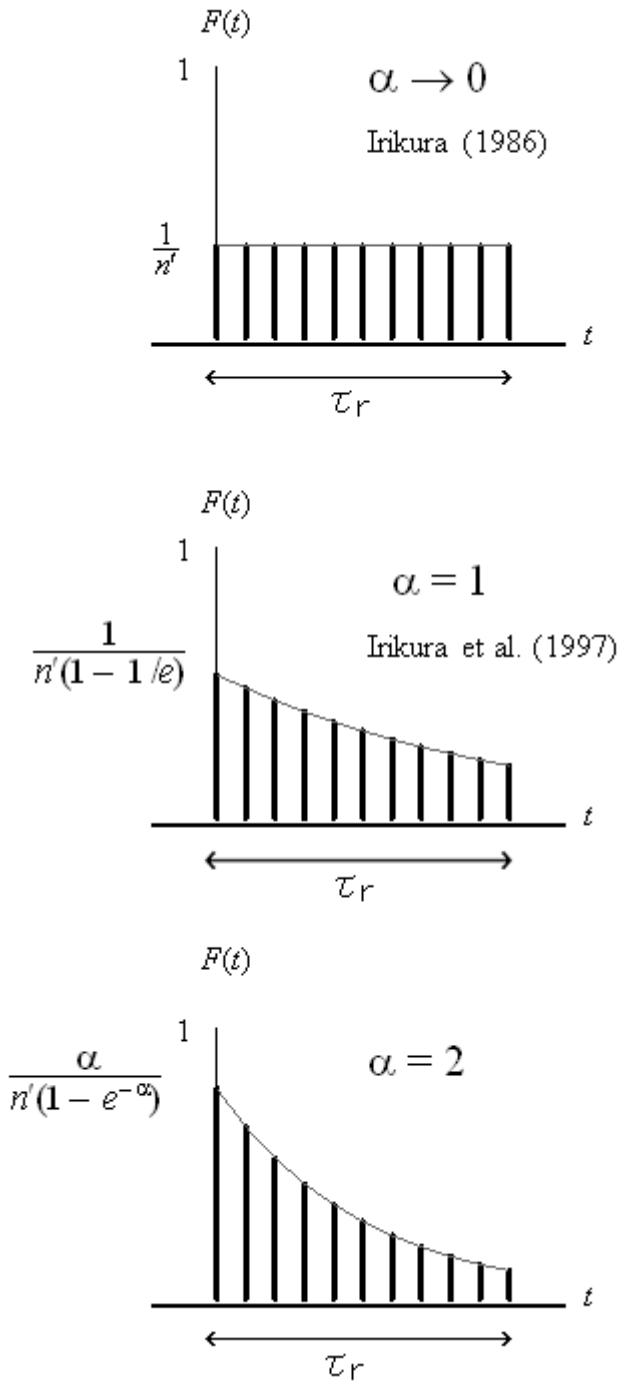

Figure 4 Schematic illustrations of the correction function F(t) in Equation (19) corresponding to various α values. If α approaches to zero, F(t) approaches to the correction function of Irikura (1986). When α equals to one, F(t) corresponds to the correction function of Irikura et al. (1997).

In Irikura et al. (1997)'s superposition method, Equation (16) is replaced by

$$F(t) = \delta(t) + \frac{1}{n'(1-e^{-1})} \sum_{k=1}^{(N_D-1)n'} e^{-t_k/\tau_r}\delta(t-t_k) \tag{18}$$

The correction function was further generalized by Nozu (2002) as

$$F(t) = \delta(t) + \frac{\alpha}{n'(1-e^{-\alpha})} \sum_{k=1}^{(N_D-1)n'} e^{-\alpha t_k/\tau_r}\delta(t-t_k) \tag{19}$$

If we put $\alpha = 1$ in Equation (19), then we have Equation (18). If we take the limit of $\alpha \to 0$ in Equation (19). then we have Equation (16), because the following approximation for small x holds.

$$1 - e^{-x} \cong x \tag{20}$$

The correction function F(t) in Equation (19) corresponding to various α values is schematically illustrated in Figure 4.

The intention to use Equation (16), (18) or (19) is to control the amplification factor for Step1. In fact, by using Equation (16), (18) or (19) in Step1, the Green's function is amplified by a factor of N_D in the low frequency range and by a factor of one in the high frequency range. This can be proved as follows. It should be noted that the convolution operation involved in Step1 is nothing more than a multiplication in the frequency domain. Thus, we can investigate the amplification factor in Step1 by studying the Fourier amplitude spectrum of the correction function (16), (18) or (19). We use Equation (19), because it is a general equation.

If we take the Fourier transform of Equation (19) we have

$$\hat{F}(\omega) = 1 + \frac{\alpha}{n'(1-e^{-\alpha})} \sum_{k=1}^{(N_D-1)n'} e^{-\alpha(k-1)/(N_D-1)/n'} e^{-i\omega(k-1)\tau_r/(N_D-1)/n'}$$

$$= 1 + \frac{\alpha}{n'(1-e^{-\alpha})} \sum_{k=1}^{(N_D-1)n'} e^{-(\alpha+i\omega\tau_r)(k-1)/(N_D-1)/n'}$$

If we put

$$A = e^{-(\alpha+i\omega\tau_r)/(N_D-1)/n'}$$

and

$$M = (N_D-1)n'$$

we have

$$\hat{F}(\omega) = 1 + \frac{\alpha}{n'(1-e^{-\alpha})}\sum_{k=1}^{M} A^{k-1}$$

$$= 1 + \frac{\alpha}{n'(1-e^{-\alpha})}\frac{1-A^{M}}{1-A}$$

$$= 1 + \frac{\alpha}{n'(1-e^{-\alpha})}\frac{1-e^{-(\alpha+i\omega\tau_r)}}{1-e^{-(\alpha+i\omega\tau_r)/(N_D-1)/n'}}$$

Because *n'* is a sufficiently large integer, we can apply the approximation in Equation (20) and we have

$$\hat{F}(\omega) \cong 1 + \frac{\alpha(N_D-1)}{(1-e^{-\alpha})}\frac{\left(1-e^{-(\alpha+i\omega\tau_r)}\right)}{(\alpha+i\omega\tau_r)} \tag{21}$$

In the low frequency limit

$$\lim_{\omega\to 0}\hat{F}(\omega) = N_D$$

At high frequencies,

$$\frac{\left(1-e^{-(\alpha+i\omega\tau_r)}\right)}{(\alpha+i\omega\tau_r)}$$

involved in the second term of the right-hand side decreases with increasing ω, because, in the complex plane, the numerator is plotted on a circle with a center at (1, 0) and with a radius $e^{-\alpha}$ and its absolute value fluctuates around one, while the amplitude of the denominator increases with increasing ω. Thus, at high frequencies, the first term becomes predominant and $|\hat{F}(\omega)|$ approaches to one. Numerical examples of $|\hat{F}(\omega)|$ for different α values are shown in Figure 5.

Thus, in the superposition operation of Irikura (1986) and Irikura et al. (1997), the amplification factor is N_D in the low frequency range and one in the high frequency range in Step1. In Step2, when contributions from subfaults are summed up, the amplification factor is $N_L \times N_W$ for low frequencies where a coherent summation applies, while the amplification factor is $(N_L \times N_W)^{1/2}$ for high frequencies where a random summation applies. Therefore, if we choose $N_L = N_W = N_D = n$ as is generally done, the total amplification factor is n^3 for low frequencies and n for high frequencies as summarized in Table 1. This is the basis for the notion that the superposition operation of Irikura (1986) and Irikura et al. (1997) follows the ω^{-2} model. It should be noted, however, that the notion is valid only for the amplification factors at low and high frequency limits; the synthetic Fourier spectrum does not necessarily follow the ω^{-2} model in the intermediate frequency range as shown in the next chapter.

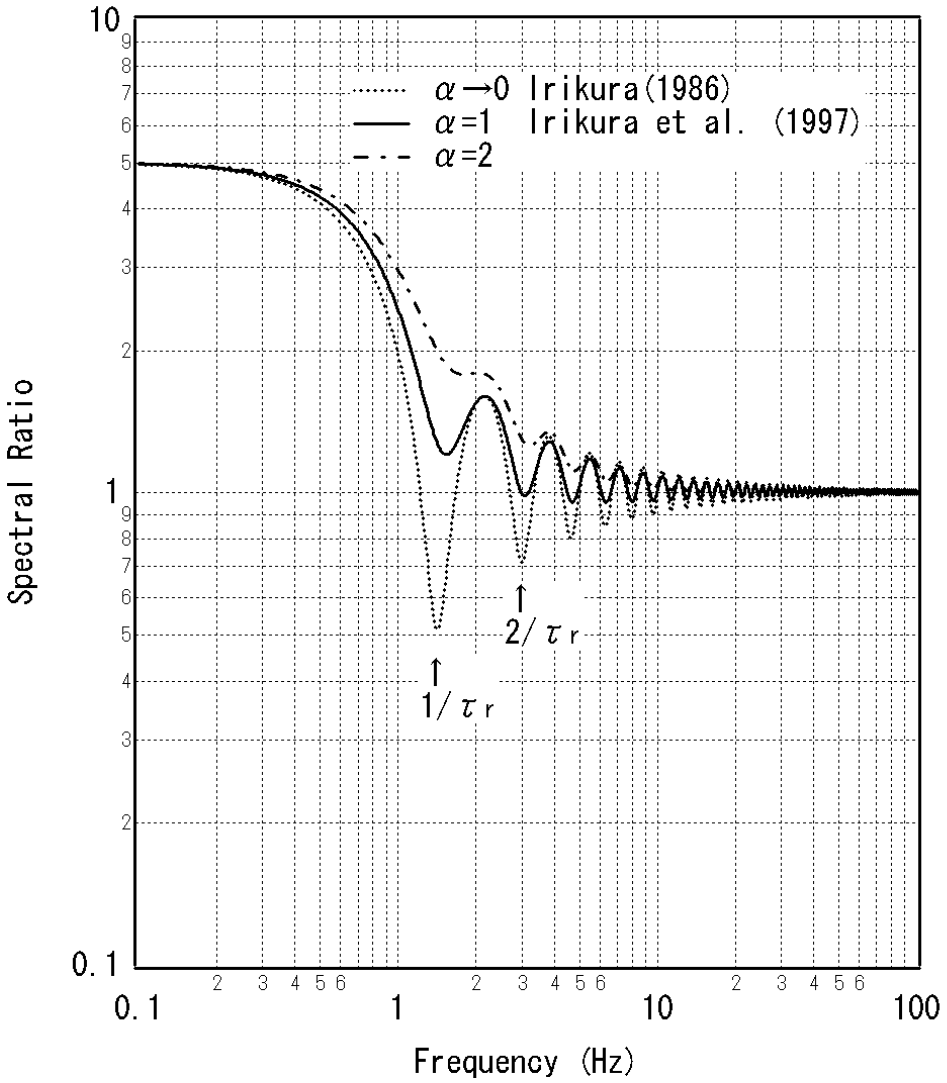

Figure 5 Numerical examples of $|\hat{F}(\omega)|$ for different α values. In this example, τ_r=0.6 s, N_D =5 and n'=100.

Table 1 Amplification factors at low and high frequencies in the superposition method by Irikura (1986) and Irikura et al. (1997)

	Low frequencies	High frequencies
Amplification in Step1	n	1
Amplification in Step2	n^2	n
Total Amplification	n^3	n

5. Spectral fall-off in the intermediate frequency range

One of the major problems associated with the application of the empirical Green's function method is that the synthetic Fourier spectrum shows a quite evident fall-off in the frequencies between the corner frequencies of the large and small events. In this chapter, the cause of the spectral fall-off is investigated.

Figure 6 shows the rectangular fault model and the receivers considered in this chapter. A rectangular fault with an area of 8×8 km^2 is embedded in a homogeneous medium with a density of 2.7×10^3 kg/m^3 and a shear-wave velocity of 3.2 km/s. The rupture initiates at the center of the fault and propagates radially at a velocity of 2.8 km/s. A uniform final slip of 1.2 m is assumed. The rise time is also uniform and it is 1.2 s.

Figure 7 shows a comparison among the synthetic spectra with the EGF method for n=5, 25 and 80 at the receiver A, the ω^{-2} target spectrum and the theoretical spectrum. The spectra are normalized so that their value is one at ω=0. The target spectrum was obtained from Equations (12) and (15), where the area for the large event was used. The synthetic spectra were obtained by the method proposed by Irikura et al. (1997), that is, Equations (8), (10) and (18). The spectrum for the small event was determined based on Equation (12), where $S(0)$ for the small event was determined by dividing $S(0)$ for the large event by n^3 and f_c for the small event was determined by multiplying f_c for the large event with n. It should be noted that the convolution operation involved in Equation (8) is nothing more than a multiplication in the frequency domain. So, we don't need Fourier phase information for the small event to calculate the synthetic spectra. The theoretical spectrum was obtained by numerically evaluating the integral in Equation (2). The fault was divided into 10000×10000 elements. The following slip velocity time function was used in Equation (2), because it is implied by the correction function in Equation (18) when N_D is sufficiently large:

$$\dot{D}(t) = \frac{D_0}{\tau_r(1 - e^{-1})} e^{-t/\tau_r} \tag{22}$$

where D_0 is the final slip.

The discrepancy between the synthetic spectra with the EGF method and the ω^{-2} target spectrum is evident in the intermediate frequency range especially when n is large. It should be noted that, in the frequency range where the spectral fall-off occurs, the synthetic spectra with the EGF method exactly traces the theoretical spectrum, which shows the ω^{-3} decay. Thus, the cause of the spectral fall-off is simply that, when n is sufficiently large, the synthetic spectra follow the theoretical spectrum which decays faster than the target spectrum.

The example presented here indicates that using a large n does not necessarily lead to a good result in the application of the empirical Green's function method, unlike in the finite element analysis. In practice, $n \cong 5$ is often used. In the future, the optimal n value for use in the EGF method should be found based on strong motion database.

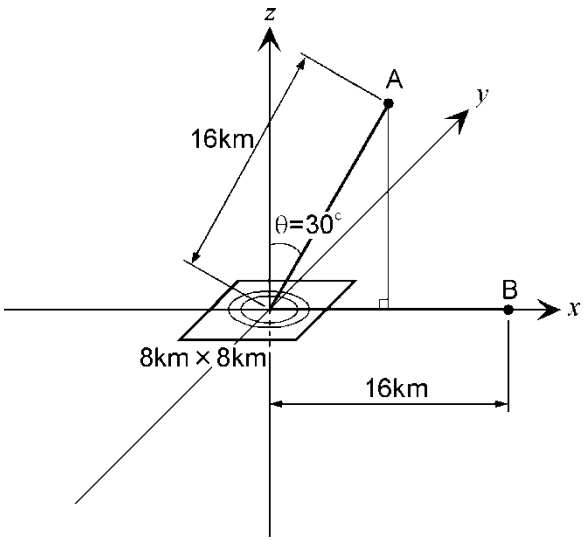

Figure 6　A schematic diagram showing the rectangular fault model, the receivers (A and B) and the coordinate system. The rupture initiates at the center of the rectangle and propagates radially at a constant rupture velocity v_r.

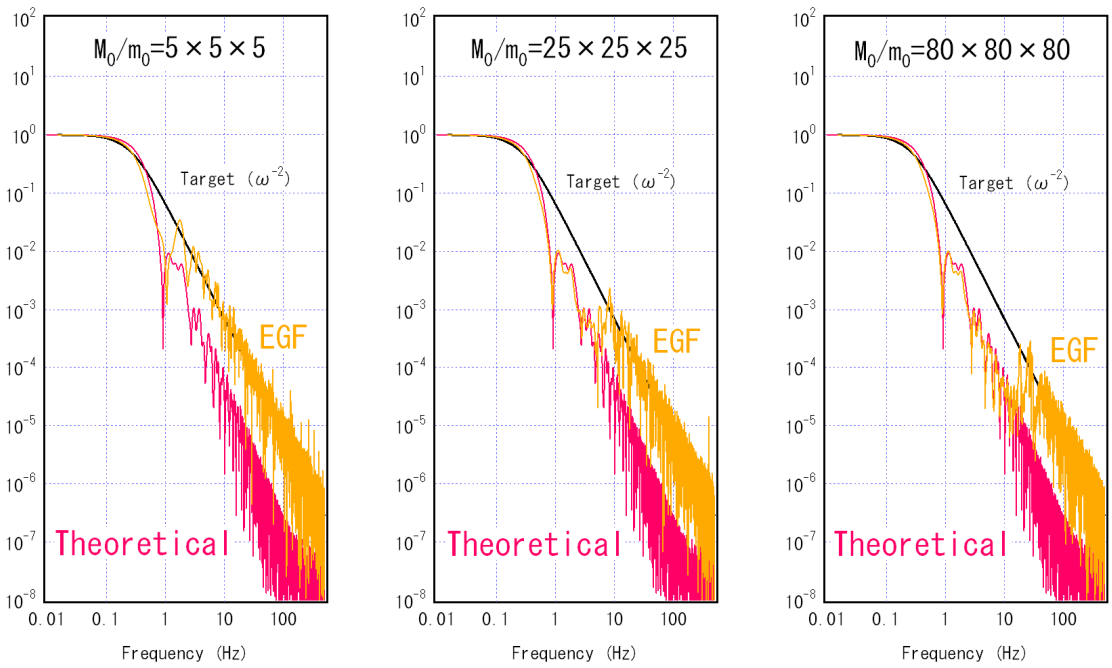

Figure 7　A comparison among the synthetic spectra with the EGF method for n=5, 25 and 80 at the receiver A (yellow), the ω^{-2} target spectrum (black) and the theoretical spectrum (red). The spectra are normalized so that their value is one at ω=0. The target spectrum was obtained from Equations (12) and (15), where the area for the large event was used. The synthetic spectra were obtained by the method proposed by Irikura et al. (1997). The theoretical spectrum was obtained by numerically evaluating the integral in Equation (2).

References

Aki, K. (1967): Scaling law of seismic spectrum, J. Geophys. Res., 72, 1217-1231.

Aki, K. and P.G. Richards (2002): Quantitative Seismology, Second Edition, University Science Books, Sausalito, California.

Brune, J. (1970): Tectonic stress and the spectra of seismic shear waves from earthquakes, J. Geophys. Res., 75, 4997-5009.

Brune, J. (1971): Correction, J. Geophys. Res., 76, 5002.

Irikura, K. (1983): Semi-empirical estimation of strong ground motions during large earthquakes, Bull. Disas. Prev. Res. Inst., Kyoto Univ., Vol.33, Part 2, No.298, pp.63-104.

Irikura, K. (1986): Prediction of strong acceleration motions using empirical Green's function, Proceedings of the 7th Japan Earthquake Engineering Symposium, pp.151-156.

Irikura, K., T. Kagawa and H. Sekiguchi (1997): Revision of the empirical Green's function method by Irikura (1986), Seismological Society of Japan Fall Meeting, No.2, B25 (in Japanese).

Nozu, A. (2002): Necessity for a generalized expression of slip velocity correction function for use in empirical Green's function method, Zisin, Vol.55, pp.233-238 (in Japanese).

Nozu, A. (2004): An application of circular crack model for empirical Green's function method, Zisin, Vol.56, pp.337-350 (in Japanese with English abstract).

Nozu, A. and K. Irikura (2008): Strong-motion generation areas of a great subduction-zone earthquake: waveform inversion with empirical Green's functions for the 2003 Tokachi-oki earthquake, Bulletin of the Seismological Society of America, Vol.98, No.1, pp.180-197.